https://doi.org/10.5194/hess-2019-225
Preprint. Discussion started: 20 June 2019

Hydrology and Earth System Sciences
Open Access
Discussions

Revisiting extreme precipitation amounts over southern South America and implications for the Patagonian Icefields

Tobias Sauter[1]

[1]Climate System Research Group, Institute of Geography, Friedrich-Alexander-University Erlangen-Nürnberg (FAU), Germany

Correspondence to: Tobias Sauter (tobias.sauter@fau.de)

Abstract. Patagonia is thought to be one of the wettest regions on Earth, although available regional precipitation estimates vary considerably. This uncertainty complicates understanding and quantifying the observed environmental changes, such as glacier recession, biodiversity decline in fjord ecosystems and enhanced net primary production. The observed dramatic volume loss of the Patagonian Icefields, for example, contradicts the reported positive surface mass balances. Here I use simple physical arguments to test the plausibility of the current precipitation estimates and its impact on the Patagonian Icefields. The results show that environmental conditions required to sustain a mean precipitation amount exceeding 6.09±0.64 m yr^{-1} are untenable according to the regional moisture flux. The revised precipitation values imply a significant reduction in surface mass balance of the Patagonian Icefields compared to previously reported values. This yields a new perspective on the response of Patagonia's glaciers to climate change and their sea-level contribution and might also help reduce uncertainties in the change of other precipitation-driven environmental phenomena.

1 Introduction

Patagonia's weather and climate are largely shaped by baroclinic eddies, which are characterized by the interaction of the planetary waves with the mean flow (Garreaud, 2009; Garreaud et al., 2013; Schneider et al., 2003; Vallis et al., 2014). The same mesoscale eddies efficiently transfer water vapor from the tropics poleward (Schneider et al., 2010; Trenberth et al., 2005), and regularly (every 9-12 days) trigger narrow filaments of water-vapor-rich bursts called atmospheric rivers. These features temporarily increase the vertical integrated water vapor content (IWV) in the Southern Hemisphere mid-latitudes by more than 200% (Durre et al., 2006; Waliser and Guan, 2017). More than half of all extreme precipitation events (above the 98th percentile) in Patagonia are associated with land-falling atmospheric rivers (Waliser and Guan, 2017). Given the tight coupling between atmospheric moisture transport and hydroclimatic response, changes in moisture transport mechanisms not only dominate the inter-annual and multi-decadal precipitation variability in Patagonia (Aravena & Luckman, 2009; Garreaud, 2007; Garreaud & Muñoz, 2005; Muñoz & Garreaud, 2005; Schneider & Gies, 2004; Viale & Garreaud, 2015; Weidemann et al., 2013; Weidemann et al., 2018), but also dictate the fate of the ice masses in this region.

https://doi.org/10.5194/hess-2019-225
Preprint. Discussion started: 20 June 2019

Hydrology and Earth System Sciences
Open Access
Discussions

The Andes constitute an effective barrier to the impinging moist tropospheric air masses, forming one of the most extreme climatic divides found worldwide (Barrett et al., 2009; Garreaud, 2009; Garreaud et al., 2013; Rasmussen et al., 2007; Smith & Evans, 2007). The strong orographic influence on the precipitation distribution is evident from both remote sensing (Wentz et al., 1998) and terrestrial observations (Fig. 1). Despite observational uncertainty along the coast, two characteristic precipitation regions are apparent: (i) a maritime pre-cordillera region with annual precipitation exceeding 2-3 m w.e. (water equivalent), and (ii) a semi-arid rain-shadow region (< 0.5 m w.e.) east of the main ridge that extends several thousand kilometres towards the South Atlantic. However, little is known about precipitation along the main ridge and, in particular, on the Patagonian Icefields. Current estimates from firn cores (Schwikowski et al., 2006; Shiraiwa et al., 2002), discharge measurements (Escobar, 1992) and numerical modelling (Bravo et al., 2019; Lenaerts et al., 2014; Mernild et al., 2017; Schaefer et al., 2013, 2015; Weidemann et al., 2018a) suggest average annual precipitation rates of 5 to 8 m w.e. yr^{-1}, and of 7 to >10 m w.e. yr^{-1} for the Northern and Southern Patagonian Icefield (NPI, SPI), respectively. Extreme precipitation rates of up to 30 m w.e. yr^{-1} are suspected at isolated locations (Lenaerts et al., 2014; Mernild et al., 2017; Schaefer et al., 2013, 2015; Schwikowski et al., 2006). If these precipitation magnitudes are realistic, it is likely that the SPI is one of the wettest – if not *the* wettest – places on earth.

The considerable uncertainty in precipitation amounts in Patagonia not only affects our current understanding of the local hydrological cycle, but also has profound impacts on studies concerned with fjord ecosystems (Landaeta et al., 2012), biological production in water columns (Aracena et al., 2011; Vargas et al., 2018), net primary production (Jobbágy et al., 2002), glacier mass balance (Escobar, 1992; Foresta et al., 2018; Lenaerts et al., 2014; Mernild et al., 2017; Schaefer et al., 2013, 2015; Schwikowski et al., 2006; Shiraiwa et al., 2002; Willis et al., 2012) and its contribution to sea level rise (Malz et al., 2018; Marzeion et al., 2012; Rignot et al., 2003). Reducing the plausible range of precipitation rates is a key step towards improved process understanding of such systems and offers new perspectives on future changes.

Here I use simple physical scaling arguments and a linear modelling approach to test the plausibility of the current precipitation estimates in central Patagonia (45°S-52°S). In particular, I address the question of whether the water vapor flux (WVF) from the tropics to the mid-latitudes by baroclinic eddies can sustain these extreme precipitation estimates. The assessment of the hypothesis relies on three fundamental assumptions: (i) The orographically induced precipitation is proportional to the incoming WVF which acts as the major moisture resource for the precipitation system. This implies that uncertainties in the incoming WVF directly impact the precipitation estimate. (ii) The terrain forced uplift and condensation of moist air masses is assumed to be the dominant precipitation formation process in central Patagonia. This criterion requires a stably stratified atmospheric flow, more precisely given by a positive moist buoyancy frequency. During the study period from 2010 to 2016, the condition was fulfilled in more than 99% of all days. As a part of this assumption, the approach also requires a linear mountain flow response, to guarantee that the airflow crosses the mountain range. The linearity requirement was met in 82% of the cases (see Sec. 3.4). (iii) The atmospheric drying ratio derived from observed isotope data is a valid measure for the

Hydrology and Earth System Sciences
Open Access
Discussions

cross-mountain fractionation of the WVF. Based on this assumption, the proposed methods are constrained by the DR to accurately reproduce the fraction of the water vapor flux removed by orographic precipitation.

After a description of the methods (Sec. 2), the moisture transport in southern South America is explored in more detail (Sec. 3.1). The chapter begins with the analysis of the available atmospheric soundings and compares them with remote sensing products and reanalysis data. Following this, the knowledge gained from the experiments on local precipitation formation (Sec. 3.2) and its implications for the surface mass balance of the SPI (Sec. 3.3) will be discussed and critically reviewed (Section 3.4). The last section provides a conclusion of the main findings.

2 Methodology

To provide a first assessment of the magnitude of precipitation, mean precipitation is estimated along the western slopes of the Andes (45°-52°S and 73°-76°W) using a simple DR- scaling. The DR in Patagonia, defined as the fraction of the WVF removed by orographic precipitation, is known to be the highest (~0.45-0.5) worldwide (Mayr et al., 2018; Smith & Evans, 2007). The ratio is a characteristic measure for mountain ranges and is independent of the incoming WVF. As the WVF and the DR (here we use 0.45) are known from ERA-Interim data and isotope observations (Langhamer et al., 2018; Mayr et al., 2018; Smith & Evans, 2007), one can estimate the mean homogeneous (uniform) precipitation amount. To add altitude-dependent precipitation variability, the amount was redistributed mass-consistently by optimizing (Newton-Raphson algorithm) the vertical precipitation gradient. The precipitation at sea level was determined from the GPM measurements offshore of the Chilean coast (~3 m yr^{-1}). The optimization resulted in a vertical precipitation gradient of 0.00052 m m^{-1} (~0.02% m^{-1}), which represents a slightly smaller lapse rate than previously reported (Schaefer et al., 2013). This approach converts the entire specified WVF fraction into precipitation regardless of the saturation vapor deficit of the impinging air masses. However, orographic precipitation can only occur when the terrain forced uplift and cooling of air masses lead to water vapor condensation. To take this condition into account, only lower tropospheric (below 950 hPa) air masses are considered with a relative humidity equal to or exceeding 90% (Jarosch et al., 2012; Weidemann et al., 2013). The DR-scaling provides a first-order approximation but neglects heterogeneity and important processes such as airflow dynamics and cloud physics.

To account for these aspects, a set of realistic and extreme ensemble experiments has been designed using a linear orographic precipitation model, which represents many processes using relative simple formulations for airflow dynamics and cloud physics (Garreaud et al., 2016; Jarosch et al., 2012; Smith and Barstad, 2004; Smith and Evans, 2007; Weidemann et al., 2018a). The model builds upon the original formulation of the linear orographic precipitation model (Smith and Barstad, 2004), including a correction of the WVF downstream (Smith and Evans, 2007) and an optimization to enforce the model towards a given drying ratio. It solves two steady-state advection equations describing the condensation of water vapor by terrain forced uplift and conversion from cold water to hydrometeors. Mountain wave theory allows for decay of the vertical velocity caused

https://doi.org/10.5194/hess-2019-225
Preprint. Discussion started: 20 June 2019

by tilting mountain waves, and consequently constrains the water vapor condensation rate. Assuming horizontal uniform background flow and properties, the orographic precipitation can be represented by a transfer function that can be solved in Fourier space. The parsimonious model contains five parameters, an uplift sensitivity factor C_w, the moist buoyancy frequency N_m^2, the water vapor scale height H_w, and the condensation and fallout time scales τ_c and τ_f. The total precipitation field is obtained by adding up the orographic precipitation from the orographic precipitation model and the background precipitation caused by the synoptic-scale uplift. For consistency, the latter one is calculated by removing the orographic component from the ERA-Interim precipitation field (Jarosch et al., 2012). To enforce the model towards a given drying ratio DR_{def}, the background precipitation is scaled by a constant, so that the calculated DR corresponds to DR_{def}. The model is solved on a 90 m SRTM dataset, resampled at 1 km resolution (Jarvis et al., 2008). The mean horizontal wind velocities (U, V) and the parameters C_w and N_m^2 are calculated from 6-hourly ERA-Interim fields (2010-2016) below the 500 hPa geopotential level off Patagonia's west coast between 48°-52°S and 75°-78°W (Fig. 1, D1). On contrary to most other studies, H_w is directly de rived from the incoming WVF using $H_w = WVF/(\rho q_w U)$, where q_w is the total mixing ratio and ρ the air density. The time scales of $\tau_c = \tau_f = 850$ s are fixed for all experiments, which are realistic values for Southern Andes and produce remarkable similar results to numerical models (Garreaud et al., 2016; Smith and Evans, 2007).

The orographic precipitation model is used to conduct a suite of ensemble experiments with 40 ensemble members. The ensembles members account for the initial condition uncertainty in the wind direction and moisture content by randomly perturbing U (5%), V (5%), and H_w (10%) around its mean value. In the first experiment, it was tested whether a composite of 'realistic' atmospheric ambient conditions (derived from the reanalysis data), the observed drying ratio of 0.45 (Mayr et al., 2018) and WVF provides the basis to sustain the precipitation estimates of previous studies. The second experiment deliver an 'extreme' scenario by fixing the drying ratio at a higher value of 0.6 and setting the uplift sensitivity factor ($C_w = 0.004$) and moist stability frequency ($N_m = 0.007$) to their 98th percentile values.

3 Results and Discussion

3.1 Moisture transport

Observations of IWV and WVF are sparse in South America and limits the analysis of the moisture transport to a few locations (see Fig. 2). The only available soundings for the region are Puerto Montt (41.4347°S, 73.0975°W) on the Pacific coast and Punta Arenas (53.0033°S, 70.8450°W) located at the Strait of Magellan (Durre et al., 2006). Along the coast, the average WVF is about 165.52±48.51 kg m^{-1} s^{-1}. Land-falling atmospheric rivers temporarily amplify the WVF by more than 400 kg m^{-1} s^{-1}. There is also clear evidence that enhanced atmospheric circulation during strong El Niño events (Ocean Niño Index >1.5) increase the moisture flux over several months. The El Niño signal is less pronounced in Punta Arenas. The atmospheric soundings show opposite linear long-term WVF trends over the period 1990-2016 with a significant (p<0.08) decrease of -

4.46 kg m^{-1} s^{-1} (-2.70%) decade^{-1} in Puerto Montt, and a significant ($p<0.05$) positive trend of 8.79 kg m^{-1} s^{-1} (5.11%) decade^{-1} in Punta Arenas (see Fig. 2). However, change-point analysis shows that the observed WVF trend in Punta Arenas is not constant over time, but has shown significant abrupt shifts in the past that characterize the transition of water vapor rich and poor periods (Killick et al., 2012). A significant transition took place in 2006 which marks the beginning of a relative water vapor rich period (Fig. 2).

The ERA-Interim data, on which the analysis is based, reflects the interannual variability and overall trend of the soundings but slightly overestimates the rate of change in Puerto Montt (-4.94 kg m^{-1} s^{-1} decade^{-1}, -4.43% decade^{-1}), and underestimates the observed trend in Punta Arenas (4.10 kg m^{-1} s^{-1} decade^{-1}, 2.70% decade^{-1}). The mean WVF at both sites is weaker than the observed moisture transport. In Puerto Montt, the WVF is about 111.54±34.40 kg m^{-1} s^{-1}, which is almost 30% less than the estimate from the atmospheric sounding. The differences between observed WVF (172.12±54.19 kg m^{-1} s^{-1}) and reanalysis data (152.08±57.08 kg m^{-1} s^{-1}) is much lower in Punta Arenas. The comparison with SSMIS data over the ocean confirms the north-south pattern (see supporting information Fig. S2). While IWV differences between ERA-Interim data and SSMIS south of 45°S are on average smaller than 0.16 mm (1.1%), larger deficits are apparent north of 45°S (<-0.8 mm). Based on the comparison with the atmospheric soundings and SSMIS observation, ERA-Interim underestimates the IWV along the west coast of Patagonia (D1 in Fig. 1), where the corresponding parameters for the assessment were calculated, by less than 5%. However, comparison with the soundings suggest that the WVF in the ERA-Interim data along the west coast is weaker by 10-20%. In the following analysis, a WVF bias of 10% is assumed and corrected accordingly.

3.2 Physical constraints on local precipitation

To obtain the plausible range of precipitation amounts in central Patagonia, the DR-scaling and the linear model are driven by the ERA-Interim data for the period 2010-2016. The DR-scaling results in a mean precipitation rate of 3.45±0.14 m yr^{-1} in the Pre-Cordillera region, with maximum values of 4.89±0.97 m yr^{-1}. Averaged over the SPI and NPI, this approach produces values of 5.46±1.30 m yr^{-1} and 5.38±1.26 m yr^{-1}, respectively (Table 1). The highest peaks on the icefields receive precipitation amounts of up to 9.63±3.69 m yr^{-1}.

The orographic precipitation model is applied to a large domain (Fig. 1, D2) to avoid spurious numerical artefacts. The ensemble mean of the realistic experiment (DR=0.45) gives an average precipitation amount of 5.06±0.51 m yr^{-1} over the SPI and 5.38±0.59 m yr^{-1} over the NPI (Table 1, Fig. 3), indicating that the WVF can sustain relatively high mean precipitation amounts in Patagonia. While these values agree with precipitation estimates derived from water discharge measurements (Escobar, 1992) and ice core stable isotopes records (Schwikowski et al., 2006), they are up to 38% lower than estimates from previous numerical studies (Lenaerts et al., 2014; Schaefer et al., 2013, 2015). The highest mean amounts are found on the windward side of the icefields (6.95±0.70 m yr^{-1}) and at the southernmost end of the SPI. The leeward slopes receive considerably less precipitation (4.04±0.42 m yr^{-1}). The spatial pattern on the plateau is consistent with the observed elevation

https://doi.org/10.5194/hess-2019-225
Preprint. Discussion started: 20 June 2019

Hydrology and Earth System Sciences Discussions

gain from radar interferometric measurements (Malz et al., 2018). Comparison with in-situ observations from the Dirección de General de Aguas (DGA, Chile) indicates that the model slightly overestimates precipitation on the leeward side by 0.29±0.37 m yr^{-1} (see Table S2). Greater deviations (1.07±1.30 m yr^{-1}) occur at the stations on the west side which are located at the foot of the Patagonian Icefields. The overestimation is the result of the rapid increase in model terrain elevation and the absence of nonlinear processes in the linear model (see Sec. 3.4). The maximum precipitation amount (10.09±0.92 m yr^{-1}), found on the SPI plateau, is ~30-70% lower than previously simulated extremes (Lenaerts et al., 2014; Schaefer et al., 2013, 2015; Shiraiwa et al., 2002). The large ensemble spread indicates that extreme precipitation is very sensitive to small uncertainties in ambient flow conditions. Even though the uncertainty in the background flow regime and dynamics may also be a possible origin of the extreme precipitation predicted by the mesoscale models, the responsible mechanisms explaining the significant differences remain unclear.

The extreme experiment shows higher averaged precipitation amounts of 5.99±0.59 m yr^{-1} and 6.09±0.64 m yr^{-1} at the SPI and NPI, respectively (Fig. 3). The combination of short time scales, large drying ratio, strong moist stability frequency, and large uplift sensitivity factor increases the total precipitation and enhances the cross-mountain fractionation. Despite the precipitation-enhancing parameter choices, the maximum precipitation (11.58±0.98 m yr^{-1}) represents a reduction of up to 60% compared to other numerical studies (Lenaerts et al., 2014; Schaefer et al., 2013, 2015). In addition, the estimated maximum is presumably an overestimate itself, due to the 'extreme' parameter choice and to the exclusion of nonlinear effects, such as flow blocking (see Sec. 3.4), given the linear nature of the orographic model.

3.3 Consequences of revised precipitation estimates on the surface mass balance of the SPI

These revised precipitation estimates have critical implications for our current understanding of the response of Patagonia's glaciers to climate change. Recent numerical studies (Mernild et al., 2017; Schaefer et al., 2015) suggest a mean annual surface mass gain of 1.78±0.36 m to 2.24 m w.e. yr^{-1} for the SPI over recent decades, while surface mass balance (SMB) estimates for the NPI range between -0.16±0.73 m w.e. yr^{-1} and 0.14±0.49 m w.e. yr^{-1}. However, these assessments used mean precipitation rates well above (40-65%) the plausible range presented in this study.

To quantify the effect of the revised precipitation values on the SMB, we use the significant linear relation (R^2=0.96, $p<0.05$) between precipitation and SMB (see Fig. 4), which follows $SMB=1.2588 \cdot P_S-3.9355$, where P_S is the mean solid precipitation. (Schaefer et al., 2013, 2015). Taking into account the proposed solid to total precipitation ratio of 0.596 (Schaefer et al., 2015), the mean solid precipitation is 3.02±0.30 m w.e. (realistic scenario) and 3.57±0.35 m. w.e. (extreme scenario) for the SPI. Based on this assumption, the revised accumulation values would result in a mean SMB between 0.56±0.45 m w.e. yr^{-1} (7.82±6.28 km^{-3} yr^{-1}) and -0.14±0.39 m w.e. yr^{-1} (-1.95±5.45 km^{-3} yr^{-1}) on the SPI (Fig. 4). The SMB estimate from the DR-scaling is within these limits. Taking account of the recent geodetic mass balance observations (-0.941±0.19 m w.e.) (Malz et

https://doi.org/10.5194/hess-2019-225
Preprint. Discussion started: 20 June 2019

al., 2018), the mean mass loss due to calving ranges between -1.5±0.64 (-20.95±8.94 km^{-3} yr^{-1}) and -0.8±0.58 m. w.e. yr^{-1} (-11.18±8.10 km^{-3} yr^{-1}). The SMB and calving flux might be even smaller when considering snowdrift effects.

Given the strong link between glacier SMB and the local hydrological cycle, the long-term SMB evolution scales with the strength of the WVF, which is, in turn projected to increase in a warming climate. The WVF sensitivity along Patagonia's west coast (~50°S) is on the order of ~15% K^{-1} (~3% decade^{-1}) as a result of the strengthening of the westerlies (~20% K^{-1}) and increase in IWV (~5% K^{-1}) south of 45°S. The latter is weaker than the change in global-mean IWV which scales according to the Clausius-Clapeyron relation (7% K^{-1}) but is consistent with the assumption that increased latent heat flux is compensated by the sensible heat flux (Held et al., 2006; Schneider et al., 2010). The observed zonal wind trend is associated with a bias towards a more positive Antarctic annular mode (Garreaud et al., 2013; Marshall et al., 2017; Thompson & Solomon, 2002). The change of the WVF leads to stronger moisture flux convergence along the coastal zone west of the Andes main ridge. Ignoring the fact that the solid-liquid ratio changes, which appears to be a reasonable assumption since temperature changes in the lower troposphere are negligible (~0.01 K dec^{-1}), a mean mass gain of 0.57±0.06 m w.e. per degree warming (0.11±0.02 m w.e. decade^{-1}) is expected over the SPI. This rate is consistent with other studies (Mernild et al., 2017). Thus, although the precipitation values presented here indicate that present-day SMB of the SPI is likely not as positive as suggested by previous studies, SMB can be expected to show an increasing trend under continued warming conditions.

3.4 Limitations and nonlinearities

In view of the linear nature of the approach used, the knowledge gained must be critically assessed and is only valid under certain conditions. A necessary requirement is the linear mountain flow response. To ensure a linear flow regime, the non-dimensional mountain height $\widehat{H} = (N_m\, h_m)/U$ must be smaller than one, where h_m is the mean barrier height. Assuming a mean $h_m = 2200$ m, the conditions ($\widehat{H} < 1$) is fulfilled in >82% of all considered cases (see Fig. 5). In the remaining cases ($\widehat{H} \geq 1$), the Andes block the atmospheric flow, and a northerly low-level barrier jet forms along the west slope, parallel to the main ridge (Barrett et al., 2009; Falvey and Garreaud, 2007; Garreaud and Muñoz, 2005; Viale and Garreaud, 2015) (see Fig. 6). The low-level jet constitutes an effective barrier to the flow that extends upwind, greatly reducing the uplift motions and thus the condensation of water vapor along the west slopes. The shift in the vertical uplift enhances precipitation upstream of the Andes, while reducing precipitation at the slopes. The effect of blocking is clearly evident in the precipitation fields of high-resolution (500 m) atmospheric simulations using the Weather Research and Forecast (WRF) model (see Fig. 7 and Table S3). Two water-vapor-rich events were chosen to illustrate the influence of the flow regime on the spatial distribution of precipitation. While the linear flow regime has a pronounced precipitation maximum on the slopes, flow blocking shifts the precipitation far upstream (600-700 km) leading to a more homogeneous pattern.

https://doi.org/10.5194/hess-2019-225
Preprint. Discussion started: 20 June 2019

Upstream precipitation can be further enhanced by microphysical processes such as the seeder-feeder mechanism and rapid warm air autoconversion. Studies have shown that these processes can lead to higher rain accumulations upstream when fronts and embedded atmospheric rivers intersect the west coast of central Chile (Garreaud et al., 2016; Massmann et al., 2017; Viale et al., 2013; Viale and Garreaud, 2015). The lifting of moist air masses upstream produces mid-tropospheric stratiform clouds (seeder) which can be strong enough to produce snow/graupel aloft and light precipitation in the pre-frontal region. If the frontal system is slowed down by blocking, low-level convergence enhances in the area of the narrow cold-frontal rainband and fuels the updrafts. The enhanced updrafts facilitate the development of low-level clouds by collision-coalescence between supercooled droplets. When the narrow cold frontal rainband propagates further east it triggers the seeder-feeder mechanism and low-tropospheric clouds are seeded by the precipitation that is formed by mid-tropospheric clouds aloft. The associated rapid transformation of cloud water into hydrometeors and increased hydrometeor sizes are absent in the approach presented. Here, the process is treated simplistic by the choice of small time scales and by constraining the synoptic-scale uplift (background precipitation). This solution most likely lead to (i) an overestimation of precipitation on the west slopes of the SPI, (ii) an underestimation of precipitation in the Pre-Cordillera zone, but (iii) satisfies the given DR_{def} constraint. Compliance with the DR criterion is the necessary condition to verify the plausibility of precipitation estimates.

4 Conclusion

The present study has shown on the basis of simple physical arguments that it is very unlikely that the moisture flux from the Pacific will be sufficient to sustain the reported extreme mean precipitation amounts for Patagonia. While the approaches and assumptions employed in this study contain substantial uncertainties, precipitation estimates using other parameter combinations fall within the range between the realistic and the extreme scenario. Hence, this study offers a plausible range of precipitation estimates on the basis of clearly defined assumptions. The values within this range are about 40-65% lower than previously assumed. Extreme precipitation in wind-exposed regions is in the range of 11.58±0.98 m yr^{-1}, ~30-50% lower than estimated by other numerical studies (Lenaerts et al., 2014; Schaefer et al., 2013, 2015; Shiraiwa et al., 2002). It should also be noted that processes such as snowdrift and nonlinear effects have not been taken into account so that the actual accumulation rates are probably still below these estimates. This result makes it very unlikely that Patagonia is the wettest place on Earth. More importantly, the drier hydroclimatic condition represents a major constraint for the Patagonian Icefields and reduces the precipitation contribution to the glacier mass balance. The missing contribution is clearly evident in the surface mass balance. According to the results, the average SMB was between 0.56±0.45 m w.e. yr^{-1} (7.82±6.28 km^{-3} yr^{-1}) and -0.14±0.39 m w.e. yr^{-1} (-1.95±5.45 km^{-3} yr^{-1}) in the last decades. On the long-term, the regional precipitation is likely to increase by ~15% per degree warming in response to stronger moisture flux. Assuming that changes in the orographically induced precipitation is proportional to the moisture changes, the WVF changes would result in a glacier surface mass gain of about 0.57±0.06 m w.e. per degree warming. This positive trend contradicts the recently published geodetic mass balance observations (Malz et al., 2018), which detected quick glacier recessions in these regions. The observed retreat is significantly stronger than the gain in ice mass implying that the ice mass budget is partially decoupled from the climate signal and primarily caused by dynamic adjustments of tidewater and lake calving glaciers. The pronounced dynamic glacier response emphasizes that ice dynamic processes need to be given more prominence in order to quantify the response of the Patagonian glaciers to climate change and their contribution to future sea-level rise. While the change in ice masses is a vivid example of the response to reduced precipitation, it also opens new perspectives for future studies on environmental change in Patagonia and can also help reduce uncertainties in the quantification of other precipitation-driven environmental phenomena.

Acknowledgments, Samples, and Data

This work was supported by the German Research Foundation (DFG), no. SA 2339/4-1. I would like to thank Manuel Gebetsberger, Emily Collier, Thomas Mölg, and Nicolas Cullen for the discussion and support. The simulations were calculated on the High-Performance Cluster (HPC) at the Regional Computation Center (RRZE) of the University of Erlangen-Nürnberg.

Data and materials availability: Data were obtained from the European Centre for Medium-Range Forecast (ECMWF), the National Aeronautics and Space Administration (NASA), Consortium for Spatial Information (CGIAR-CSI), and Integrated Global Radiosonde Archive (IGRA) from the National Centers for Environmental Information (NCEI).

References

Aracena, C., Lange, C. B., Iriarte, J. L., Rebolledo, L. and Pantoja, S.: Latitudinal patterns of export production recorded in surface sediments of the Chilean Patagonian fjords (41-55 S) as a response to water column productivity, Cont. Shelf Res., 31(3–4), 340–355, 2011.

Aravena, J. C. and Luckman, B. H.: Spatio-temporal rainfall patterns in Southern South America, Int. J. Climatol., 29, 2106–2120, doi:10.1002/joc, 2009.

Barrett, B. S., Garreaud, R. and Falvey, M.: Effect of the Andes Cordillera on Precipitation from a Midlatitude Cold Front, Mon. Weather Rev., 137(9), 3092–3109, doi:10.1175/2009MWR2881.1, 2009.

Bravo, C., Bozkurt, D., Gonzalez-Reyes, Á., Quincey, D. J., Ross, A. N., Farías-Barahona, D. and Rojas, M.: Assessing Snow Accumulation Patterns and Changes on the Patagonian Icefields, Front. Environ. Sci., 7, 30, doi:10.3389/fenvs.2019.00030, 2019.

Durre, I., Vose, R. S. and Wuertz, D. B.: Overview of the integrated global radiosonde archive, J. Clim., 19(1), 53–68, doi:10.1175/JCLI3594.1, 2006.

Escobar, F.: Water balance in the Patagonia Icefield, Glaciol. Res. Patagon. 1990, 109–119, 1992.

Falvey, M. and Garreaud, R.: Wintertime Precipitation Episodes in Central Chile: Associated Meteorological Conditions and

Orographic Influences, J. Hydrometeorol., 8(2), 171–193, doi:10.1175/JHM562.1, 2007.

Foresta, L., Gourmelen, N., Weissgerber, F., Nienow, P., Williams, J. J., Shepherd, A., Drinkwater, M. R. and Plummer, S.: Heterogeneous and rapid ice loss over the Patagonian Ice Fields revealed by CryoSat-2 swath radar altimetry, Remote Sens. Environ., 211, 441–455, 2018.

Garreaud, R., Falvey, M., Montecinos, A., Garreaud, R., Falvey, M. and Montecinos, A.: Orographic Precipitation in Coastal Southern Chile: Mean Distribution, Temporal Variability, and Linear Contribution, J. Hydrometeorol., 17(4), 1185–1202, doi:10.1175/JHM-D-15-0170.1, 2016.

Garreaud, R. D.: Precipitation and circulation covariability in the extratropics, J. Clim., 20(18), 4789–4797, doi:10.1175/JCLI4257.1, 2007.

Garreaud, R. D.: The Andes climate and weather, Adv. Geosci., 22, 3–11, doi:10.5194/adgeo-22-3-2009, 2009.

Garreaud, R. D. and Muñoz, R. C.: The Low-Level Jet off the West Coast of Subtropical South America: Structure and Variability, Mon. Weather Rev., 133(12), 2246–2261, doi:10.1175/MWR3074.1, 2005.

Garreaud, R. D., Lopez, P., Minvielle, M. and Rojas, M.: Large-scale control on the Patagonian climate, J. Clim., 26(1), 215–230, doi:10.1175/JCLI-D-12-00001.1, 2013.

Held, I. M., Soden, B. J., Held, I. M. and Soden, B. J.: Robust Responses of the Hydrological Cycle to Global Warming, J. Clim., 19(21), 5686–5699, doi:10.1175/JCLI3990.1, 2006.

Jarosch, A. H., Anslow, F. S. and Clarke, G. K. C.: High-resolution precipitation and temperature downscaling for glacier models, Clim. Dyn., 38(1–2), 391–409, doi:10.1007/s00382-010-0949-1, 2012.

Jarvis, A., Reuter, H. I., Nelson, A. and Guevara, E.: Hole-filled SRTM for the globe Version 4, 2008.

Jobbágy, E. G., Sala, O. E. and Paruelo, J. M.: Patterns and controls of primary production in the Patagonian steppe: a remote sensing approach, Ecology, 83(2), 307–319, 2002.

Killick, R., Fearnhead, P. and Eckley, I. A.: Optimal detection of changepoints with a linear computational cost, J. Am. Stat. Assoc., 107(500), 1590–1598, doi:10.1080/01621459.2012.737745, 2012.

Landaeta, M. F., López, G., Suárez-Donoso, N., Bustos, C. A., Balbontiín, F. and Balbontín, F.: Larval fish distribution, growth and feeding in Patagonian fjords: potential effects of freshwater discharge, Environ. Biol. Fishes, 93(1), 73–87, doi:10.1007/s10641-011-9891-2, 2012.

Lenaerts, J. T. M., Van Den Broeke, M. R., van Wessem, J. M., van de Berg, W. J., van Meijgaard, E., van Ulft, L. H., Schaefer, M. and Bilt, D.: Extreme precipitation and climate gradients in Patagonia revealed by high-resolution regional atmospheric climate modeling, J. Clim., 27(12), 4607–4621, doi:10.1175/JCLI-D-13-00579.1, 2014.

Malz, P., Meier, W., Casassa, G., Jaña, R., Skvarca, P. and Braun, M. H.: Elevation and mass changes of the Southern Patagonia Icefield derived from TanDEM-X and SRTM Data, Remote Sens., 10(2), 188, 2018.

Marshall, G. J., Thompson, D. W. J. and van den Broeke, M. R.: The Signature of Southern Hemisphere Atmospheric Circulation Patterns in Antarctic Precipitation, Geophys. Res. Lett., 44(22), 11,580-11,589, doi:10.1002/2017GL075998, 2017.

Marzeion, B., Jarosch, A. H. and Hofer, M.: Past and future sea-level change from the surface mass balance of glaciers, Cryosph., 6(6), 1295–1322, 2012.

Massmann, A. K., Minder, J. R., Garreaud, R. D., Kingsmill, D. E., Valenzuela, R. A., Montecinos, A., Fults, S. L. and Snider, J. R.: The Chilean Coastal Orographic Precipitation Experiment: Observing the Influence of Microphysical Rain Regimes on Coastal Orographic Precipitation, J. Hydrometeorol., 18(10), 2723–2743, doi:10.1175/jhm-d-17-0005.1, 2017.

Mayr, C., Langhamer, L., Wissel, H., Meier, W., Sauter, T., Laprida, C., Massaferro, J., Försterra, G. and Lücke, A.: Atmospheric controls on hydrogen and oxygen isotope composition of meteoric and surface waters in Patagonia, Hydrol. Earth Syst. Sci. Discuss., 1–22, doi:10.5194/hess-2018-431, 2018.

Mernild, S. H., Liston, G. E., Hiemstra, C. and Wilson, R.: The Andes Cordillera. Part III: glacier surface mass balance and contribution to sea level rise (1979–2014), Int. J. Climatol., 37(7), 3154–3174, doi:10.1002/joc.4907, 2017.

Muñoz, R. C. and Garreaud, R. D.: Dynamics of the Low-Level Jet off the West Coast of Subtropical South America, Mon. Weather Rev., 133(12), 3661–3677, 2005.

Rasmussen, L. A., Conway, H. and Raymond, C. F.: Influence of upper air conditions on the Patagonia icefields, , 59, 203–216, doi:10.1016/j.gloplacha.2006.11.025, 2007.

Rignot, E., Rivera, A. and Casassa, G.: Contribution of the Patagonia Icefields of South America to Sea Level Rise, Science (80-.)., 302(5644), 434–437, doi:10.1126/science.1087393, 2003.

Schaefer, M., Machguth, H., Falvey, M. and Casassa, G.: Modeling past and future surface mass balance of the Northern Patagonia Icefield, J. Geophys. Res. Earth Surf., 118(2), 571–588, doi:10.1002/jgrf.20038, 2013.

Schaefer, M., MacHguth, H., Falvey, M., Casassa, G. and Rignot, E.: Quantifying mass balance processes on the Southern Patagonia Icefield, Cryosphere, 9(1), 25–35, doi:10.5194/tc-9-25-2015, 2015.

Schneider, C. and Gies, D.: Effects of El Niño-southern oscillation on southernmost South America precipitation at 53°S revealed from NCEP-NCAR reanalyses and weather station data, Int. J. Climatol., 24(9), 1057–1076, doi:10.1002/joc.1057, 2004.

Schneider, C., Glaser, M., Kilian, R., Santana, A., Butorovic, N. and Casassa, G.: Weather Observations Across the Southern Andes at 53°S, Phys. Geogr., 24(2), 97–119, doi:10.2747/0272-3646.24.2.97, 2003.

Schneider, T., O'Gorman, P. a., Levine, X. J., Gorman, P. A. O. and Levine, X. J.: Water vapor and the dynamics of climate changes, Rev. Geophys., (48), 1–22, doi:10.1029/2009RG000302.1.INTRODUCTION, 2010.

Schwikowski, M., Brütsch, S., Casassa, G. and Rivera, A.: A potential high-elevation ice-core site at Hielo Patagónico Sur, Ann. Glaciol., 43, 8–13, 2006.

Shiraiwa, T., Kohshima, S., Uemura, R., Yoshida, N., Matoba, S., Uetake, J. and Godoi, M. A.: High net accumulation rates at Campo de Hielo Patagonico Sur, South America, revealed by analysis of a 45.97 m long ice core, Ann. Glaciol., 35(1), 84–90, 2002.

Smith, R. B. and Barstad, I.: A Linear Theory of Orographic Precipitation, J. Atmos. Sci., 61(12), 1377–1391, 2004.

Smith, R. B. and Evans, J. P.: Orographic Precipitation and Water Vapor Fractionation over the Southern Andes, J.

https://doi.org/10.5194/hess-2019-225
Preprint. Discussion started: 20 June 2019

Hydrometeorol., 8(1), 3–19, doi:10.1175/JHM555.1, 2007.

Thompson, D. W. J. and Solomon, S.: Interpretation of recent Southern Hemisphere climate change, Science (80-.)., 296(5569), 895–899, doi:10.1126/science.1069270, 2002.

Trenberth, K. E., Fasullo, J. and Smith, L.: Trends and variability in column-integrated atmospheric water vapor, Clim. Dyn., 24(7–8), 741–758, doi:10.1007/s00382-005-0017-4, 2005.

Vallis, G. K., Zurita-gotor, P., Cairns, C. and Kidston, J.: Response of the Large-Scale Structure of the Atmosphere to Global Warming, Q. J. R. Meteorol. Soc., 141(0000), 1–27, doi:10.1002/qj.2456, 2014.

Vargas, C. A., Cuevas, L. A., Silva, N., González, H. E., Pol-Holz, D., Narváez, D. A. and others: Influence of Glacier Melting and River Discharges on the Nutrient Distribution and DIC Recycling in the Southern Chilean Patagonia, J. Geophys. Res. Biogeosciences, 123(1), 256–270, 2018.

Viale, M. and Garreaud, R.: Orographic effects of the subtropical and extratropical Andes on upwind precipitating clouds, J. Geophys. Res. Atmos., 120(10), 4962–4974, 2015.

Viale, M., Houze, R. A., Rasmussen, K. L., Viale, M., Jr., R. A. H. and Rasmussen, K. L.: Upstream Orographic Enhancement of a Narrow Cold-Frontal Rainband Approaching the Andes, Mon. Weather Rev., 141(5), 1708–1730, doi:10.1175/MWR-D-12-00138.1, 2013.

Waliser, D. and Guan, B.: Extreme winds and precipitation during landfall of atmospheric rivers, Nat. Geosci., 10(3), 179–183, doi:10.1038/ngeo2894, 2017.

Weidemann, S., Sauter, T., Schneider, L. and Schneider, C.: Impact of two conceptual precipitation downscaling schemes on mass-balance modeling of Gran Campo Nevado ice cap, Patagonia, J. Glaciol., 59(218), 1106–1116, doi:10.3189/2013JoG13J046, 2013.

Weidemann, S., Sauter, T., Malz, P., Jaña, R., Arigony-Neto, J., Casassa, G. and Schneider, C.: Glacier Mass Changes of Lake-Terminating Grey and Tyndall Glaciers at the Southern Patagonia Icefield Derived From Geodetic Observations and Energy and Mass Balance Modeling, Front. Earth Sci., 6, 81, doi:10.3389/feart.2018.00081, 2018a.

Weidemann, S. S., Sauter, T., Kilian, R., Steger, D., Butorovic, N. and Schneider, C.: A 17-year Record of Meteorological Observations Across the Gran Campo Nevado Ice Cap in Southern Patagonia, Chile, Related to Synoptic Weather Types and Climate Modes, Front. Earth Sci., 6, doi:10.3389/feart.2018.00053, 2018b.

Wentz, F. J., Spencer, R. W., Systems, R. S., Rosa, S. and Hydrology, G.: SSM/I rain retrievals within a unified all-weather ocean algorithm, J. Atmos. Sci., 55(9), 1613–1627, 1998.

Willis, M. J., Melkonian, A. K., Pritchard, M. E. and Rivera, A.: Ice loss from the Southern Patagonian ice field, South America, between 2000 and 2012, Geophys. Res. Lett., 39(17), 2012.

Hydrology and Earth System Sciences
Open Access
Discussions

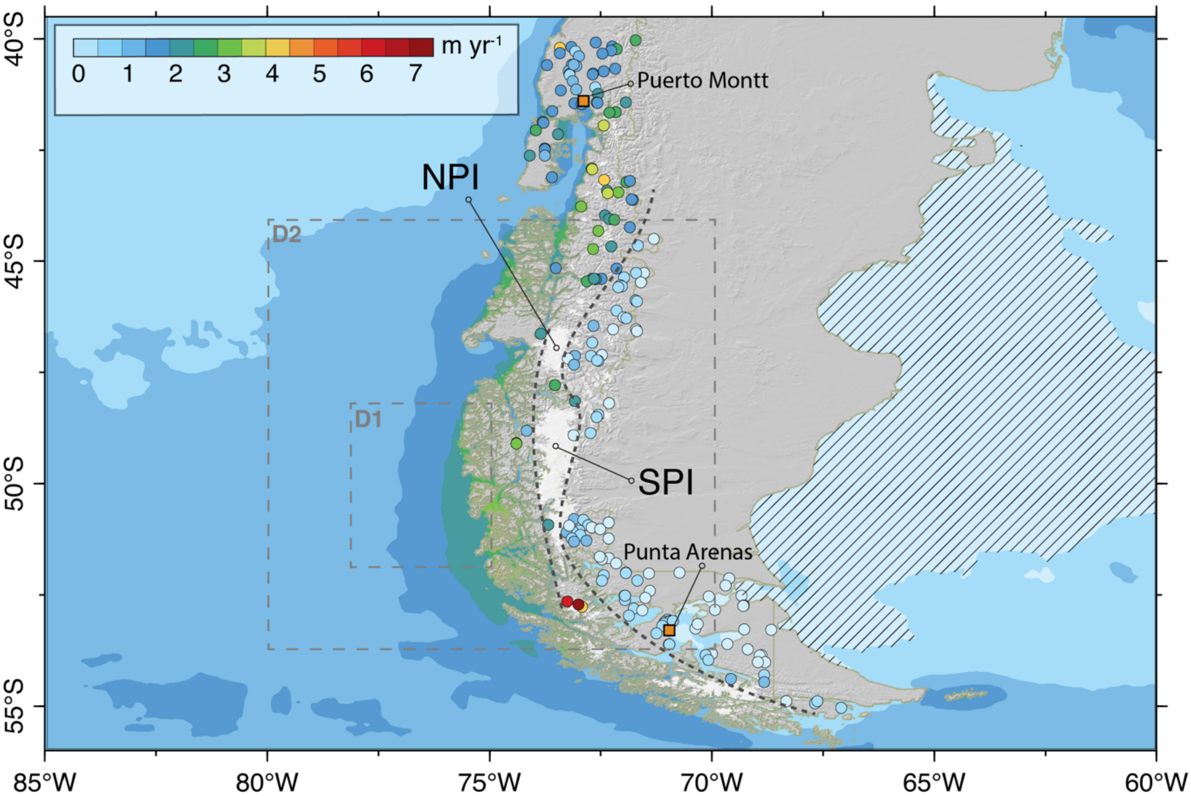

Figure 1: Precipitation climatology in southern South America. The filled circles indicate precipitation amounts measured by the observational network, established by the Dirección Meteorológica de Chile (DMC), Dirección General de Aguas (DGA), and own weather stations. The colour shaded areas over the ocean shows the rainfall distribution based on the Global Precipitation Measurement (GPM) satellite mission. Black dashed lines roughly delineate the maritime Pre-Cordillera range, Andes main ridge, and the semiarid Pampa region. Also indicated are the Northern (NPI) and Southern Patagonian Icefields (SPI). The dashed area shows the semi-arid rain-shadow region. Also shown are the simulation (D2) and forcing (D1) domains.

https://doi.org/10.5194/hess-2019-225
Preprint. Discussion started: 20 June 2019

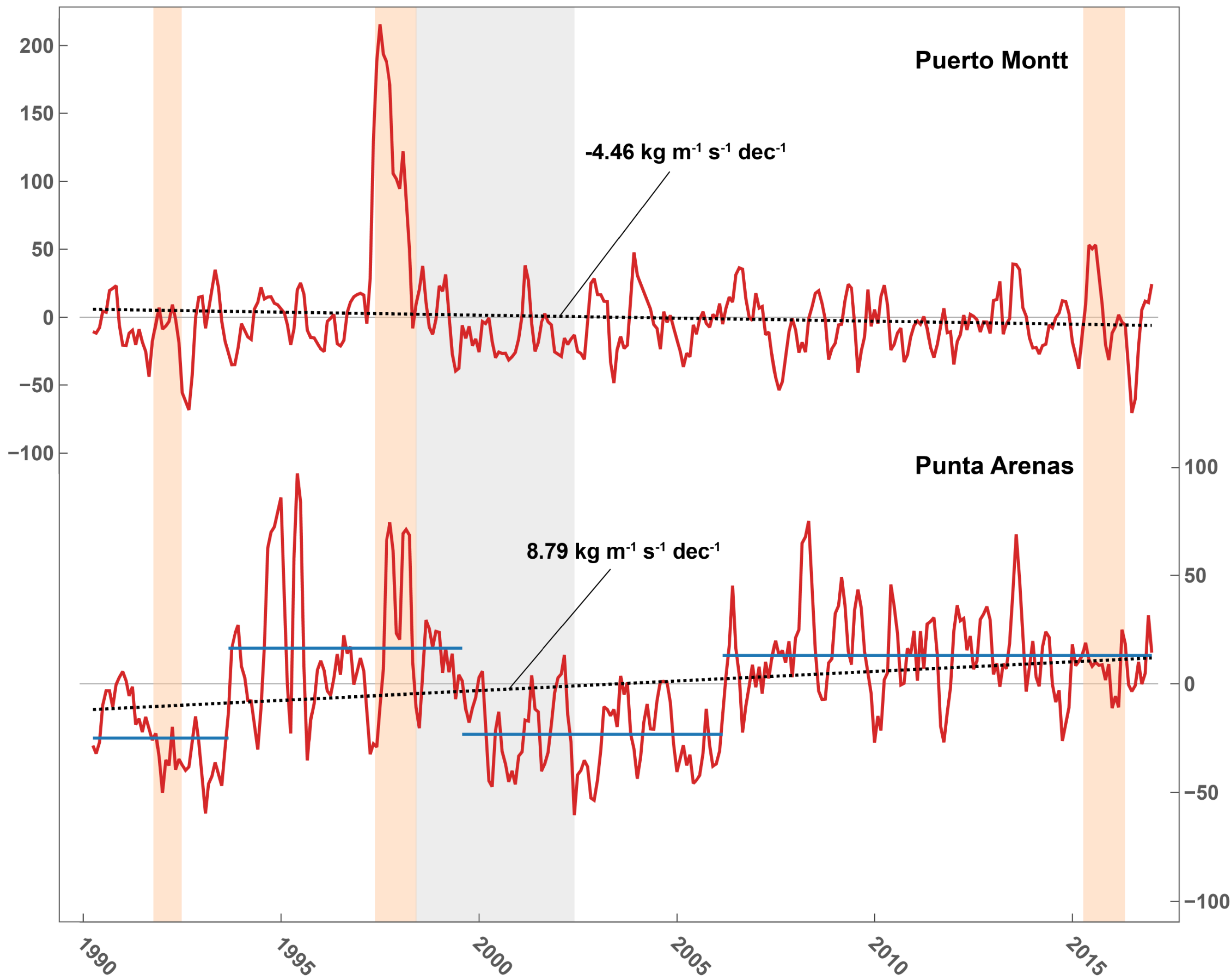

Figure 2: Monthly WVF anomalies. Atmospheric soundings for (A) Puerto Montt and (B) Punta Arenas from 1990 to 2016. The orange shaded areas indicate strong El Niño events (ONI>1.5), while the grey shaded areas indicate strong La Niña events (ONI<-1.5). The blue lines show the mean WVF over water vapor rich and poor phases.

https://doi.org/10.5194/hess-2019-225
Preprint. Discussion started: 20 June 2019

Hydrology and Earth System Sciences
Open Access
EGU
Discussions

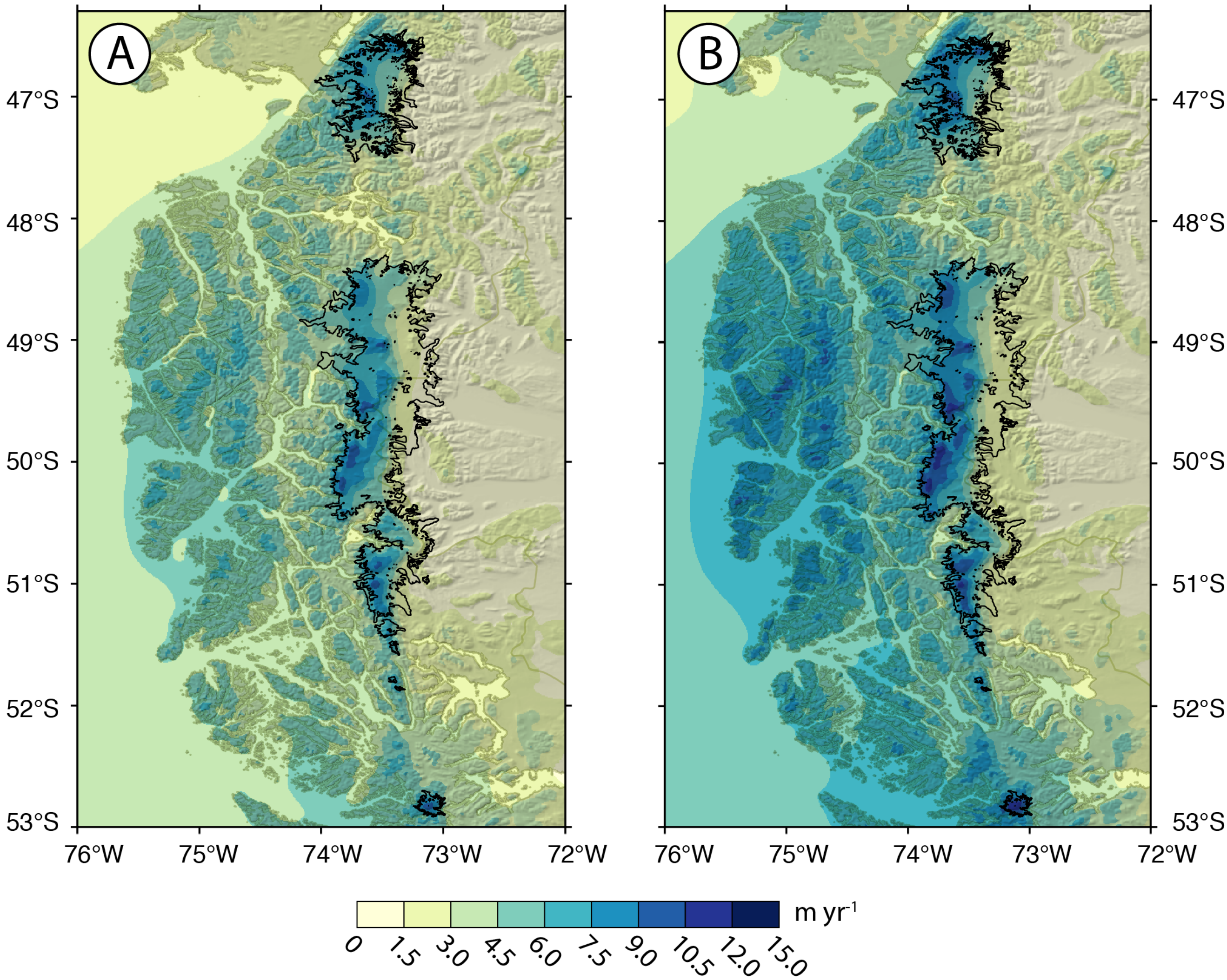

Figure 3: Results of the OPM ensemble experiments. Mean precipitation fields simulated by the OPM using (A) the 'realistic' (DR=0.45) parameter setup, and (B) the 'extreme' parameter setup using a DR of 0.6 and the 98th percentile values for the uplift sensitivity factor (Cw=0.004) and moist stability frequency (Nm=0.007).

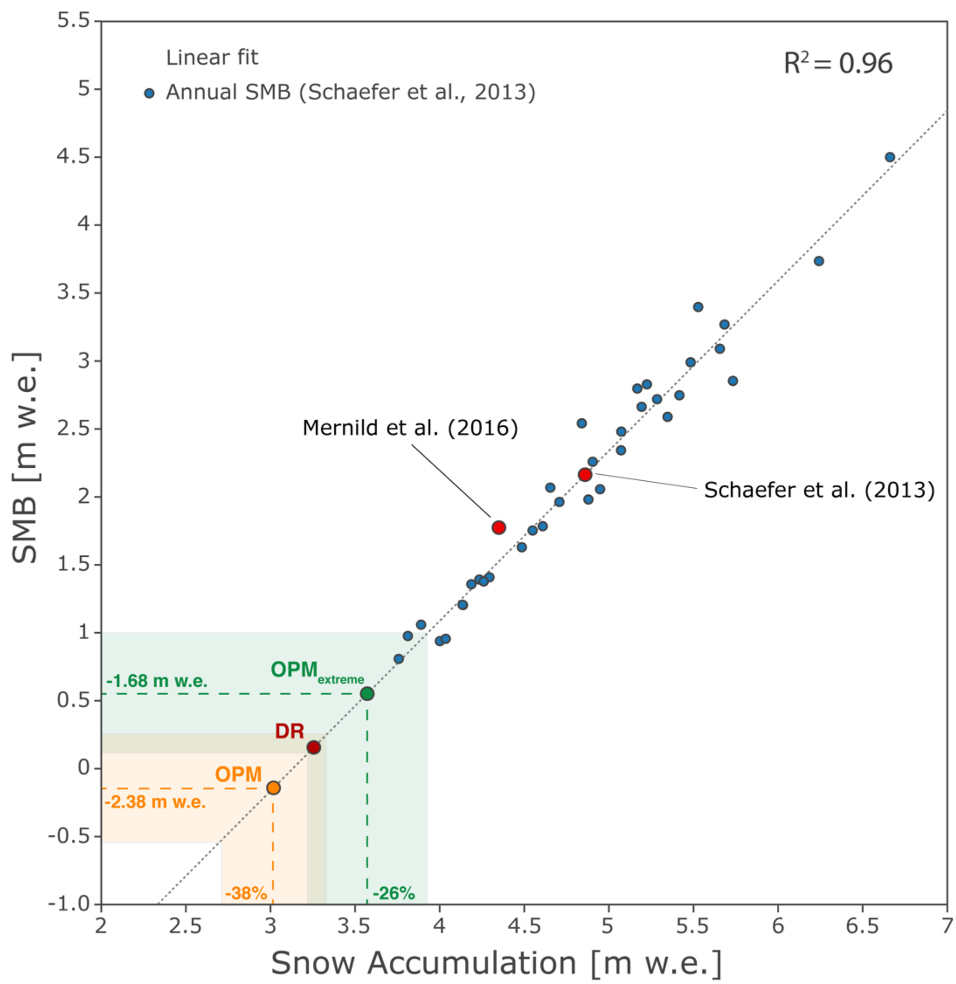

Figure 4: Relation between the annual specific accumulation and surface mass balance over the SPI from 1975-2000. The red, green and orange dots mark the multi-annual mean values using the accumulation rates from Schaefer et al. (2013), Mernild et al. (2016) and this study, respectively. The shaded areas mark lower and upper snow accumulation and SMB bounds derived from the DR-scaling (DR), the realistic (OPM) and extreme ($OPM_{extreme}$) orographic precipitation model experiments. The percentage and numbers show the differences between the current study and the values given by Schaefer et al..

https://doi.org/10.5194/hess-2019-225
Preprint. Discussion started: 20 June 2019

Hydrology and Earth System Sciences
Discussions

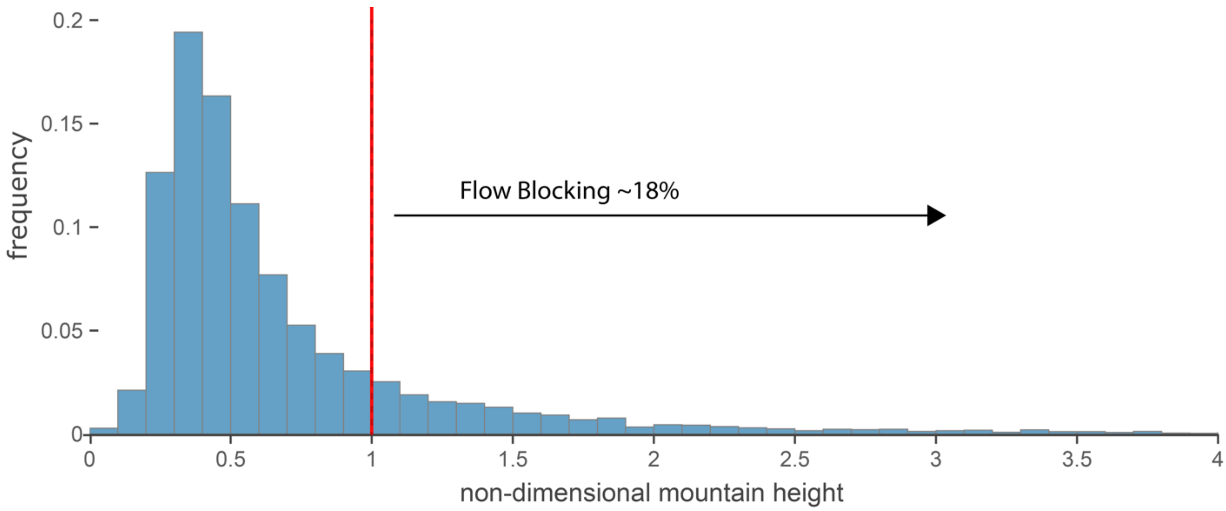

Figure 5: Frequency distribution of the non-dimensional mountain height. The non-dimensional mountain height is calculated from ERA-Interim data (2010-2016) off Patagonia's west coast (Fig. 1, D1).

https://doi.org/10.5194/hess-2019-225
Preprint. Discussion started: 20 June 2019

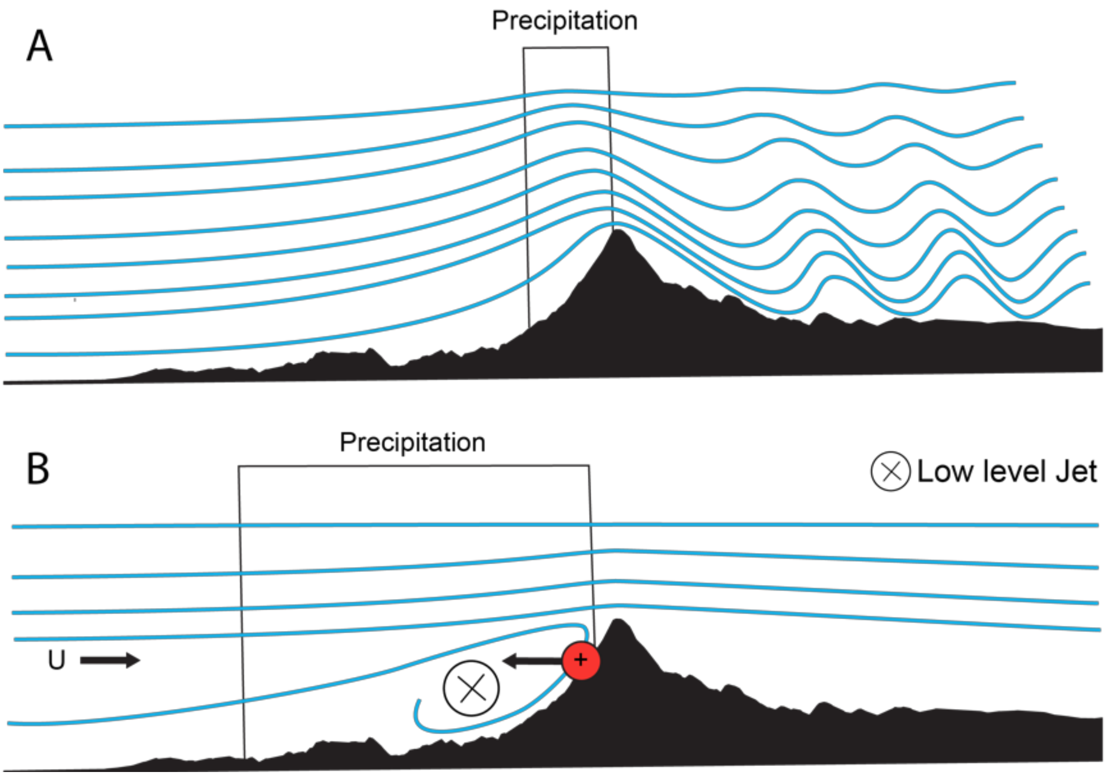

Figure 6: Schematic illustration of the interaction between the atmospheric air flow and the Andes. (A) Linear mountain flow response (Ĥ<1) leads to strong uplift and precipitation along the west slopes. (B) The air flow is blocked by the topography (Ĥ≥1) and the resulting pressure gradient (indicated by the red circle) at the west slope slows down the upstream flow. The imbalance between the large-scale pressure gradient and Coriolis-force leads to a northerly low-level jet, which reduces and shifts the uplift motions upstream. This mechanism enhances precipitation in the Pre-Cordillera range, while reducing precipitation at the west slopes of the Andes.

https://doi.org/10.5194/hess-2019-225
Preprint. Discussion started: 20 June 2019

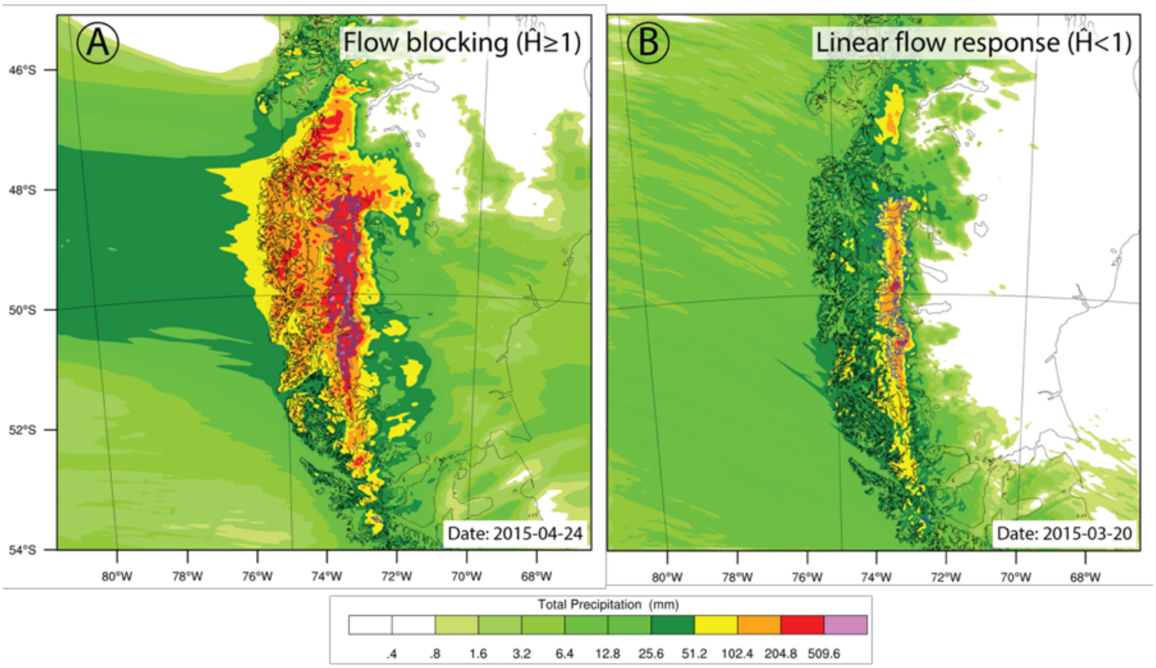

Figure 7: Total precipitation sums (3-days) over the SPI and NPI from WRF for different flow regimes. (A) Nonlinear flow response with enhanced precipitation in the Pre-Cordillera range and (B) linear flow response with strong localized precipitation along the west slopes of the Andes.

5

Hydrology and Earth System Sciences
Open Access
Discussions

Table 1: Comparison of mean precipitation estimates on the SPI and NPI. Values are given in m w.e. yr-1. The local maximum values, if available, are shown in parentheses.

	SPI	NPI	Periode
Realistic scenario (mean)	5.06±0.51 (10.09±0.92)	5.38±0.59 (9.43±0.93)	2010-2016
> 3000 m	8.03±0.81	7.16±0.79	
2500–3000 m	6.37±0.65	6.58±0.67	
2000-2500 m	5.39±0.54	5.69±0.58	
1000-2000 m	5.29±0.54	5.58±0.62	
< 1000 m	4.26±0.44	4.81±0.54	
Extreme scenario (mean)	5.99±0.59 (11.58±0.98)	6.09±0.64 (10.37±0.96)	2010-2016
> 3000 m	8.89±0.89	7.67±0.85	
2500–3000 m	7.09±0.73	7.05±0.73	
2000-2500 m	6.08±0.61	6.16±0.64	
1000-2000 m	6.19±0.61	6.21±0.67	
< 1000 m	5.34±0.53	5.74±0.58	
DR-scaling (mean)	5.46±1.30 (8.99±3.33)	5.38±1.26 (9.63±3.69)	2010-2016
Other studies			
Schaefer et al. (2015)	8.36 (>20.0)	8.03±0.37 (>15.0)	1975-2011
Mernild et al. (2016)	8.13±0.32 (>15.0)	6.95±0.34 (>15.0)	1979-2014
Lenaerts et al. (2013)	- (>10.0)	- (>30.0)	1979-2012
Escobar et al. (1992)	7.0	6.7	1960-1980